A dimensionality reduction technique for 2D scattering problems in photonics

O. V. (Alyona) Ivanova[1], Remco Stoffer[2], and Manfred Hammer[1]

[1]MESA+ Institute for Nanotechnology, University of Twente, Enschede, The Netherlands
[2]PhoeniX Software, Enschede, The Netherlands

Abstract

This paper describes a simulation method for 2D frequency domain scattering problems in photonics. The technique reduces the spatial dimensionality of the problem by means of global, continuous mode expansion combined with a variational formalism; the resulting equations are solved using a finite element method. Transparent influx boundary conditions and perfectly matched layers are employed at the computational window boundaries. Numerical examples validate the method.

Keywords: integrated optics; numerical modelling; optical scattering; variational methods
PACS: 42.82.m; 42.82.Et

1 Introduction

Photonic integrated circuit design relies in general heavily on computational tools. Simulations are, on the one hand, employed for rough and approximate, but quick and efficient assessment of a configuration. On the other hand, the verification and fine-tuning of a design requires rigorous, accurate calculations, that typically demand a much higher computational effort. Among the multitude of existing approaches to frequency domain scattering problems in photonics we will briefly highlight two methods that are typically used for the aforementioned purposes.

Although "the" Effective Index Method (EIM) is mostly being formulated for the calculation of waveguide modes [1, 2, 3, 4, 5, 6, 7], optical scattering problems can just as well be treated in terms of effective indices [8, 9, 10, 11, 12]. Replacing, more or less heuristically, the original 2D Helmholtz problem by a scalar equation for 1D frequency domain wave propagation through an effective structure, one obtains a very approximate solution at very low computational cost. In contrast, Bidirectional Eigenmode Propagation (BEP, also called Eigenmode Expansion Method or EME) schemes aim at accurate, converged solutions [3, 13, 14, 15, 16, 17]. Meant for structures with piecewise constant permittivity, the optical electromagnetic field is expanded locally into sets of 1D slab modes. Bidirectional mode overlaps then connect the local expansions across interfaces.

The current method is conceptually similar to what was applied in the context of scalar and vectorial mode solvers [18, 19] and employs a global mode expansion. A given structure is enclosed by a computational window (CW) (Figure 1, box), with metallic upper and lower boundaries that are equipped with Perfectly Matched Layers (PMLs) [20]. Then slab modes of one or more suitable vertical cross-section(s) are calculated (functions of x in Figure 1), and one assumes that a superposition of these modes gives a reasonable approximation to the true field profile everywhere on the horizontal axis y. A variational restriction procedure [21] then allows to extract a system of second order differential equations for the unknown, now only y-dependent, coefficient functions. To find a

numerical solution to this system we use a Finite Element Method (FEM) [22]. Transparent Influx Boundary Conditions (TIBCs) [23, 21, 24, 25] are implemented at the left and right boundaries of the computational domain. These permit to prescribe the given influx, while radiation from within the CW can freely pass through the left and right boundary; at the top and bottom of the CW, the PMLs make sure that scattered light is not reflected back from the boundaries.

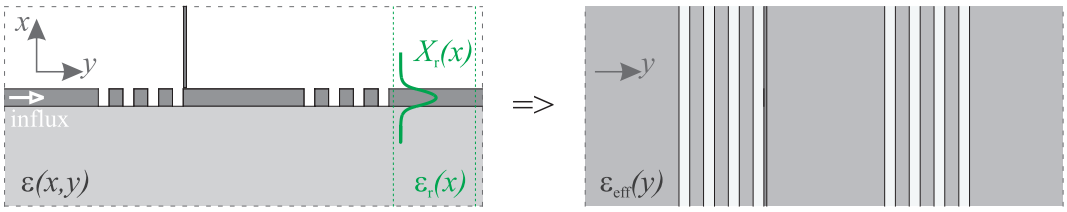

Figure 1: 2-to-1D dimensionality reduction, the defect grating structure with a probe tip from Section 3.2. Using a global mode expansion together with variational techniques, the original problem in two spatial dimensions (left) is reduced to an effective system of differential equations in one spatial variable (right).

Note that the present scheme uses an expansion basis quite similar to a conventional BEP approach. Our expansions, however, are global; continuity requirements at vertical interfaces are "automatically" satisfied. In combination with a suitable selection of basis modes, the variational procedure generates reasonable approximations already with relatively few expansion terms. As an extreme case, expansions with only one vertical mode can be viewed as a variant of an EIM. Contrary to the "standard" formulations, the present approach allows to determine uniquely the effective indices, even if a local slab does not support any guided modes. While in this paper we will only touch this particular case, more detailed remarks can be found in Ref. [12].

Apart from the EIM and BEP versions cited before, relations with the bidirectional mode propagation algorithm of Ref. [26] can be observed. Global expansions are employed there as well; the fields are expanded into Fourier series. While that standard basis allows for a highly efficient handling, apart from the special case of a locally homogeneous region the basis modes are nowhere exact solutions, such that also there a rather large number of terms might be required to generate acceptable approximations (so far, however, we did not carry out a direct comparison of efficiencies).

A brief preliminary account on our method has been given in Ref. [27]. Section 2 describes the theoretical background in detail. We restrict the formulation to TE polarization. In principle, the formalism for TM polarized fields can be established, similar to the scalar analysis of guided TM modes in Ref. [18]. Examples and explicit equations for the situation with single mode expansions are included in Ref. [12]. In Sections 2.2 and 2.3 we pay some attention to the PML related particularities of the expansion basis, and to aspects of the numerical solution. Examples for a series of 2D configurations show the validity of the method in Section 3.

2 2D scattering problems

The propagation of TE-polarized monochromatic light with vacuum wavelength λ and wavenumber $k = 2\pi/\lambda$ through a dielectric structure, defined by the permittivity distribution $\varepsilon(x, y)$, is governed by the 2D Helmholtz equation for the z-component of the electric field:

$$\Delta E_z(x, y) + k^2 \varepsilon(x, y) E_z(x, y) = 0. \tag{1}$$

Solutions of Eq. (1) can also be formally found [28] as critical points of the functional [3]

$$\mathcal{F}(E_z) = \int \left[(\nabla E_z(x, y))^2 - k^2 \varepsilon(x, y) E_z^2(x, y) \right] dx\, dy. \tag{2}$$

In the following we will use the variational formulation only. While Eqs. (1, 2) cover in principle the entire x-y-plane, practical computations have to be confined to a computational window. Then suitable boundary conditions need to be implemented, that allow any given influx to be prescribed and radiation to freely leave the computational window.

2.1 Dimensionality reduction

We assume that the true field profile can be reasonably approximated at every point on the horizontal y-axis by a superposition of 1D vertical slab modes. Typically these are modes that are supported by (one or more) vertical cross-sections. Note that each mode can, in principle, be taken from a different reference slab waveguide, although in practice, many (or all) may come from the same one. Then the principal field component E_z is expanded as

$$E_z(x,y) = \sum_{j=1}^{m} X_j(x) \cdot Y_j(y), \tag{3}$$

where X_j is the principal component of a TE polarized mode from a reference slab waveguide, and Y_j is an unknown coefficient function which determines the amplitude of this mode at every position y.

By restricting the functional (2) to the set of functions in the form (3), and taking variations with respect to all unknowns Y_j, we find [18] the following system of second order differential equations for the functions Y_j:

$$\mathbf{F}\mathbf{Y}''(y) + \mathbf{M}(y)\mathbf{Y}(y) = 0. \tag{4}$$

Here $\mathbf{Y}$ is a vector function formed of all functions Y_j, and $\mathbf{F}$ and $\mathbf{M}$ are matrices of dimension $m \times m$ with elements that are given by overlap integrals involving the modes X_j, their derivatives, and the permittivity $\varepsilon(x,y)$:

$$F_{g,h} = \int X_g(x) X_h(x)\, dx, \tag{5}$$

$$M_{g,h}(y) = \int \left[k^2 \varepsilon(x,y) X_g(x) X_h(x) - X_g'(x) X_h'(x)\right] dx. \tag{6}$$

Beyond (4), for a structure divided into slices, the stationarity of (2) amounts to interface conditions of continuity of

$$\mathbf{Y}(y) \quad \text{and} \quad \mathbf{Y}'(y). \tag{7}$$

Thus, through the approximation (3), the problem of finding the function $E_z(x,y) : \mathbb{R}^2 \to \mathbb{C}$ has been reduced to the task of identifying a vector function $\mathbf{Y}(y) : \mathbb{R} \to \mathbb{C}^m$.

2.2 Basis modes X_j defined using Perfectly Matched Layers

Before we proceed to the actual solution procedure for the problem (4) in Section 2.3.1, we will introduce some short remarks on the the basis modes together with the implementation of transparency for the upper and lower computational window boundaries.

2.2.1 Perfectly matched layers

If one would use only Dirichlet boundary conditions at the top and bottom window boundaries (Figure 1), light that is scattered from the structure and reaches these boundaries would be completely reflected back into the window. In order to model an open domain, first along the x-axis, we employ the well-known Perfectly Matched Layers (PMLs) [29, 30]. Although there are other viewpoints on PMLs, we prefer to see them in the following way: In these artificial layers, the

coordinate is 'stretched' into the complex plane, providing — at least analytically — absorption of the light without causing reflections at the interior-PML boundary. We will use PMLs that act as absorbers along the x direction, where inside the PML the coordinate x is transformed as

$$x \to x - \mathrm{i} \int_0^x \sigma(\tilde{x})\, d\tilde{x}, \tag{8}$$

meaning that dx and $\dfrac{\partial}{\partial x}$ are transformed in the following way:

$$dx \to (1 - \mathrm{i}\,\sigma(x))\, dx, \qquad \frac{\partial}{\partial x} \to \frac{1}{1 - \mathrm{i}\,\sigma(x)} \frac{\partial}{\partial x}. \tag{9}$$

Let's consider how a plane wave behaves in a PML. Under the given transformations, a wave that would propagate with x-dependence $\exp(-\mathrm{i}\,k_x x)$ in non-PML media will instead behave as $\exp(-\mathrm{i}\,k_x(x - \mathrm{i}\int_0^x \sigma(\tilde{x})\, d\tilde{x})$ – i.e. if σ is positive, it is attenuated in the positive x direction. Similarly, a wave with x-dependence $\exp(\mathrm{i}\,k_x x)$ in non-PML media, inside the PML is attenuated in the negative x-direction. The consequence of this is that if a PML is placed just before a totally reflecting boundary, waves impinging on the boundary are first attenuated while traversing the PML toward the boundary, reflected, and subsequently attenuated once more. This double attenuation makes PMLs very powerful as absorbing boundary conditions in simulations of Maxwell's equations.

The parameter $\sigma(x)$, sometimes called the PML strength, equals zero outside the PML. Inside the PML, we choose it to increase linearly from zero at the interior-PML interface, to a maximum value σ_{max} at the outer boundary of the domain. The reason for a slow increase in $\sigma(x)$ is that even though the PML is analytically reflectionless, numerically a quick spatial variation of the PML strength can cause some reflections.

2.2.2 1D slab modes with PMLs

In the presence of PMLs that absorb in the x-direction, the modified Helmholtz equation (1) is

$$\left(\partial_{yy} + \frac{1}{1 - \mathrm{i}\,\sigma(x)} \partial_x \frac{1}{1 - \mathrm{i}\,\sigma(x)} \partial_x + k_0^2 \varepsilon(x, y) \right) E_z(x, y) = 0 \tag{10}$$

where $\sigma(x)$ is as described at the end of the previous subsection.

In case the refractive index does not depend on y, Eq. (10) permits modal solutions of the form $E_z(x, y) = X(x)\, \mathrm{e}^{-\mathrm{i}\,\beta y}$, where the complex mode profile X satisfies the equation

$$\left(\frac{1}{1 - i\sigma(x)} \partial_x \frac{1}{1 - i\sigma(x)} \partial_x + \left(k_0^2 \varepsilon(x, y) - \beta^2 \right) \right) X(x) = 0, \tag{11}$$

for a complex propagation constant β.

If we consider a domain $x \in [a, b]$ with zero Dirichlet boundary conditions $X(a) = 0$ and $X(b) = 0$, solutions X_j of the eigenvalue equation (11) are orthogonal in the following dot product [31]:

$$(u(x), v(x)) = \int_a^b u(x) v(x) (1 - \mathrm{i}\,\sigma(x)) dx. \tag{12}$$

To solve Eq. (11), we employ a standard finite element (FE) method, using a nonuniform 1D grid generated by a commercial package [22] with linear basis functions and constant coefficients in each element. The finite element scheme results in a generalized eigenvalue problem, the solutions of which approximate the eigenfunctions X_j and eigenvalues β_j^2 of Eq. (11). Using a FE scheme has the additional advantage that the overlap integrals (5), (6) become trivial to calculate.

2.2.3 Use of PMLs in the expansion

In order to use PMLs in the theory described in the sections 2 and 2.1, what is needed is to consistently apply the transformations given in Eq. (9) – which formally affect Eq. (1) and the functional (2), and consequently also the calculation of the overlap integrals in (5) and (6). Here, weighting factors as in Eq. (12) appear as the only complication required in practice.

2.3 Method of solution of the reduced problem (4)

In general an integrated optics component can have an arbitrary permittivity distribution, e.g. tapers (Figure 10) or sinusoidal gratings. In section 2.3.1 we will detail a numerical method of solution based on the Finite Element Method. Due to its general applicability and ease of implementation, will will only use this solution technique in the numerical results that will follow. At the same time for a large class of problems the system (4) could be solved semi-analytically, as we will briefly describe in section 2.3.2.

2.3.1 Finite Element Method combined with Transparent Influx Boundary Conditions

Using a Finite Element Method to solve the system of differential equations allows for more freedom in the structure than the semi-analytic method described below. For example, it can handle interfaces that do not run parallel to x or y, like tapered waveguides.

While the system (4) is defined on the whole $\mathbb{R}$, we have to restrict our finite element computations to the finite numerical window. Since we deal with influx interacting with optical structure, it is important to have proper boundary conditions that represent the correct physical properties of the exterior of the computational domain. Boundary conditions should allow influx to be prescribed and reflected fields to propagate through the boundary without reflection. For this purpose we use so-called Transparent Influx Boundary Conditions [28, 23, 24, 25, 32, 33].

As a requirement we have to choose the computational window $y \in [l, r]$ in such a way that outside of it the optical structure is invariant in the y-direction. Then we can readily write a weak formulation for the system (4) [33, 34]:

$$\begin{aligned}&\int_l^r \mathbf{V}^\top(y)\big[\mathbf{F}^{-1}\mathbf{M}(y)\mathbf{Y}(y) + \mathbf{Y}''(y)\big]\,dy \\ &-\mathbf{V}^\top(r)\big[\mathbf{Y}'(r) - \mathbf{Y}'_{\text{ext}}(r)\big] + \mathbf{V}^\top(l)\big[\mathbf{Y}'(l) - \mathbf{Y}'_{\text{ext}}(l)\big] = 0,\end{aligned} \tag{13}$$

where $\mathbf{V}$ is a continuous test vector-function defined on $y \in [l, r]$. $\mathbf{Y}_{\text{ext}}$ represents a — still to be established — solution to the system (4) outside the computational interval. Dashes indicate y derivatives, the symbol $^\top$ denotes the transpose. Note that $\mathbf{Y}$ is meant here to be defined exclusively on the interior interval $[l, r]$, and $\mathbf{Y}_{\text{ext}}$ – on the exterior regions $(-\infty, l] \cup [r, \infty)$. Where necessary, derivatives are to be taken as one-sided limits.

By requiring that Eq. (13) is satisfied for arbitrary $\mathbf{V}$, one recovers the system (4) for $y \in [l, r]$, together with continuity $\mathbf{Y}_{\text{ext}}(l) = \mathbf{Y}(l)$ and $\mathbf{Y}(r) = \mathbf{Y}_{\text{ext}}(r)$ of the functions (essential boundary conditions); and continuity $\mathbf{Y}'_{\text{ext}}(l) = \mathbf{Y}'(l)$ and $\mathbf{Y}'(r) = \mathbf{Y}'_{\text{ext}}(r)$ of the derivatives across the boundary (natural boundary conditions). Integrating by parts the term with the second derivative transforms Eq. (13) to a standard weak form, with simpler boundary terms:

$$\int_l^r \big[\mathbf{V}^\top(y)\mathbf{F}^{-1}\mathbf{M}(y)\mathbf{Y}(y) - (\mathbf{V}^\top(y))'\mathbf{Y}'(y)\big]\,dy + \mathbf{V}^\top(r)\mathbf{Y}'_{\text{ext}}(r) - \mathbf{V}^\top(l)\mathbf{Y}'_{\text{ext}}(l) = 0. \tag{14}$$

Now, the invariance along y of the permittivity distribution outside the computational domain makes it possible to construct the exterior solution $\mathbf{Y}_{\text{ext}}$ [25]. Since $\mathbf{M}$ is constant for $y < l$, a

particular solution of Eq. (4) in that region is

$$\mathbf{Y}_{\text{ext}}(y) = a\,\mathrm{e}^{\mathrm{i}\,\lambda y}\mathbf{p} \quad \text{for} \quad y < l, \tag{15}$$

where a is an arbitrary amplitude, and λ and $\mathbf{p}$ satisfy the eigenvalue problem

$$\mathbf{M}\mathbf{p} = \lambda^2\mathbf{F}\mathbf{p}. \tag{16}$$

To proceed further we look a bit closer at the properties of the matrices entering this eigenvalue problem. Alternatively to the expression (6), we can consider

$$M_{g,h}(y) = \beta_h^2 F_{g,h} + k^2 \int \big[\varepsilon(x,y) - \varepsilon_h(x)\big] X_g(x) X_h(x)\,dx, \tag{17}$$

derived from (6) using once integration by parts and the differential equation for the mode profile X_h. If it happens that the waveguide with the permittivity $\varepsilon_h(x)$ and which supports the mode profile X_h, coincides with the one that extends into the left exterior $y < l$, then to the left of the computational window $\varepsilon(x,y) = \varepsilon_h(x)$, and the second term of (17) vanishes. Thus column h of the matrix $\mathbf{M}$ is equal to column h of the matrix $\mathbf{F}$ times the square of β_h, the propagation constant of mode h. Hence the eigenvalue problem (16) permits a solution pair: eigenvalue $\lambda^2 = \beta_h^2$ and corresponding unit eigenvector $\mathbf{p}$, with an entry 1 at position h. This means that in the left exterior this particular mode X_h decouples from all other modes that enter the expansion (3) and contributes to the solution for $y < l$ as

$$E_z(x,y) = (a_1\,\mathrm{e}^{\mathrm{i}\,\beta_h y} + a_2\,\mathrm{e}^{-\mathrm{i}\,\beta_h y}) X_h(x) + \ldots\,, \tag{18}$$

with some coefficients a_1 and a_2. It implies that while all the other modes can be coupled through the non-unit eigenvectors $\mathbf{p}$, those that originally were computed for the same waveguide as the one in the left exterior, are not modified by the expansion (3). This property then makes it trivial to prescribe the influx through the computational boundary in terms of the modes of the incoming waveguide. Let us say we want to excite the optical structure by the mode X_h with amplitude q, which implies that

$$\mathbf{Y}_{\text{ext}}(y) = \sum_{s=1,\ldots,h,\ldots,m} a_s\,\mathrm{e}^{\mathrm{i}\,\lambda_s y}\mathbf{p}_s + q\,\mathrm{e}^{-\mathrm{i}\,\lambda_h y}\mathbf{p}_h \quad \text{for} \quad y < l, \tag{19}$$

with yet unknown coefficients a_s. We can rewrite this equation in matrix form by defining $\mathbf{a}$ to be a column-vector of all coefficients a_s; $\mathbf{E}(y)$ – a diagonal matrix with entries $\mathrm{e}^{\mathrm{i}\,\lambda_s y}$; and $\mathbf{P}$ – a matrix, composed by the vectors $\mathbf{p}_s$ as columns:

$$\mathbf{Y}_{\text{ext}}(y) = \mathbf{P}\mathbf{E}(y)\mathbf{a} + q\,\mathrm{e}^{-i\lambda_h y}\mathbf{p}_h. \tag{20}$$

Next, since the continuity conditions (7) require that $\mathbf{Y}_{\text{ext}}(y) = \mathbf{Y}(y)$ at $y = l$, we can express these coefficients in terms of the interior solution $\mathbf{Y}$ at the boundary:

$$\mathbf{a} = \mathbf{E}^{-1}(l)\mathbf{P}^{-1}\big[\mathbf{Y}(l) - q\,\mathrm{e}^{-\mathrm{i}\,\lambda_h l}\mathbf{p}_h\big]. \tag{21}$$

These coefficients then permit to express also the derivative of the exterior solution $\mathbf{Y}'_{\text{ext}}(l)$ in terms of the interior solution $\mathbf{Y}(l)$ at the boundary. Differentiating Eq. (19) gives

$$\begin{aligned}
\mathbf{Y}'_{\text{ext}}(y) &= \sum_{s=1,\ldots,h,\ldots,m} a_s\,\mathrm{i}\,\lambda_s\,\mathrm{e}^{\mathrm{i}\,\lambda_s y}\mathbf{p}_s - \mathrm{i}\,q\lambda_h\,\mathrm{e}^{-\mathrm{i}\,\lambda_h y}\mathbf{p}_h && (22)\\
&= \mathrm{i}\,\mathbf{P}\mathbf{\Lambda}\mathbf{E}(y)\mathbf{a} - \mathrm{i}\,q\lambda_h\,\mathrm{e}^{-\mathrm{i}\,\lambda_h y}\mathbf{p}_h && (23)\\
&= \mathrm{i}\,\mathbf{P}\mathbf{\Lambda}\mathbf{E}(y)\Big[\mathbf{E}^{-1}(l)\mathbf{P}^{-1}\big[\mathbf{Y}(l) - q\,\mathrm{e}^{-\mathrm{i}\,\lambda_h l}\mathbf{p}_h\big]\Big] - \mathrm{i}\,q\lambda_h\,\mathrm{e}^{-i\lambda_h y}\mathbf{p}_h, && (24)
\end{aligned}$$

where $\mathbf{\Lambda}$ is a diagonal matrix with diagonal entries λ_s. So at the boundary $y = l$ we have after some simplifications

$$\mathbf{Y}'_{\text{ext}}(l) = \mathrm{i}\,\mathbf{P}\mathbf{\Lambda}\mathbf{P}^{-1}\mathbf{Y}(l) - \mathrm{i}\,2q\lambda_h\,\mathrm{e}^{-\mathrm{i}\,\lambda_h l}\mathbf{p}_h. \tag{25}$$

Inserting this into the weak formulation (14), together with an analogous expression for $\mathbf{Y}'_{\text{ext}}(r)$ at the right boundary, we are finally able to restrict the weak formulation to the computational domain only, with all information about the exterior hidden inside the matrices $\mathbf{P}$ and $\mathbf{\Lambda}$.

2.3.2 Semi-analytic solution method

Due to common techniques of fabrication, many components of integrated optical devices have a piecewise constant rectangular permittivity distribution, e.g. the rectangular grating of Figure 2. This property of the device geometry results in a piecewise constant matrix $\mathbf{M}(y)$. Therefore the general solution of Eq. (4) can be written out on every interval where the permittivity is invariant in the y-direction. These local solutions then can be matched across the interfaces according to the interface conditions (7). We refer to [18, 35] for more detailed remarks on such approaches.

2.4 Relation to the effective index method

Regarding the relation between the present approach and "conventional" effective index methods, it is instructive to look at the expansion (3) with only a single term, $E_z(x, y) = X(x)Y(y)$. Here X will typically be the fundamental guided mode of a suitable reference slab (Figure 1), that is likely to represent a major part of the actual physical field. For the specific case of guided modes we can use an unbounded domain in x without PMLs. Let $\varepsilon_{\text{r}}(x)$ be the permittivity of that reference slab, and β_{r} be the propagation constant, such that X satisfies the slab mode equation

$$X''(x) + k^2\varepsilon_{\text{r}}(x)X(x) = \beta_{\text{r}}^2 X(x). \tag{26}$$

Then the system (4) reduces to the following EIM-like equation for the function Y:

$$Y''(y) + k^2\varepsilon_{\text{eff}}(y)Y(y) = 0, \tag{27}$$

with the effective permittivity

$$\varepsilon_{\text{eff}}(y) = \frac{\beta_{\text{r}}^2}{k^2} + \frac{\int(\varepsilon(x, y) - \varepsilon_{\text{r}}(x))X^2(x)\,dx}{\int X^2(x)\,dx}. \tag{28}$$

Similarly to the standard EIM, in the reference slice, where $\varepsilon(x, y) = \varepsilon_{\text{r}}(x)$, the effective permittivity is that of the mode X. However, in other slices it is modified by the difference between the local permittivity and that of the reference slice, weighted by the local intensity of the mode profile. So, contrary to the EIM, even in slices where no guided modes exist, an effective index can still be uniquely defined. Note that it may turn out that effective permittivity found from (28) is negative. We refer to [12] for a more detailed elaboration of this viewpoint, including a series of numerical examples.

3 Numerical results

The presented theory is implemented with the aid of the COMSOL Multiphysics package [22] for grid generation and for setting up the finite element equations in the y-direction; the slab modes are calculated by means of an in-house developed finite element code. This section shows and discusses results on three structures: A waveguide Bragg grating, a perturbed defect cavity in a grating, and a vertical taper. The acronym VEIM (variational effective index method) shall be used to indicate results of our approach.

3.1 Waveguide Bragg grating

The waveguide Bragg grating of Figure 2 served as a benchmark structure to compare independently developed 2D numerical codes in the COST 268 modelling task [36]. The grating is formed by etching 20 rectangular grooves into a Si_3N_4/SiO_2 slab waveguide. We are interested in the response of the waveguide grating, i.e. the relative guided wave transmission T and reflection R, for the incoming fundamental TE mode at varying vacuum wavelengths λ.

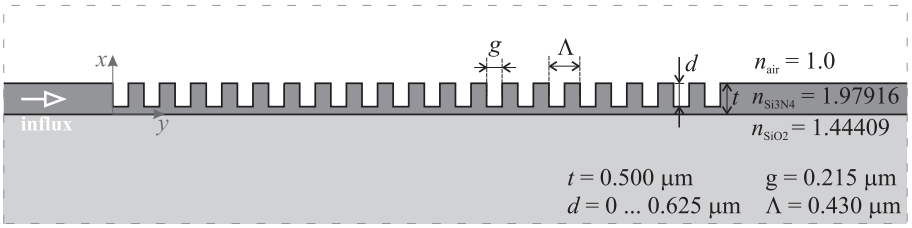

Figure 2: A waveguide Bragg grating, benchmark structure of Refs. [36] and [37].

Slab modes are calculated on a computational window $x \in [-3, 3]\mu m$ with zero Dirichlet boundaries, coated with $1\mu m$ thick PMLs, whose strength increases linearly towards the boundaries from 0 to $\sigma_{\max} = 0.8$. The expansion uses 40 slab modes of the input waveguide, which are calculated with 320 linear elements in the vertical direction. The horizontal extent $y \in [-1, 9]\mu m$ of the computational window is discretized into 352 quadratic finite elements.

Figure 3 shows a comparison of results of the present method (VEIM) to those generated by two other modelling schemes. The curves labelled QUEP are computed using the semi-analytic Quadridirectional Eigenmode Propagation scheme from Ref. [37], and the label BEP denotes results from a Bidirectional Eigenmode Propagation method with PMLs at the boundaries from Ref. [36]. The agreement between the present method and the reference results is excellent.

3.2 Waveguide Bragg grating perturbed by a nanosized probe

The authors of Ref. [38] describe a grating with a defect cavity. This structure exhibits a bandgap in which the transmission is very small, with a narrow transmission peak inside it, due to the defect. The spectrum of this cavity resonance can be shifted in wavelength, while also being deformed, by the presence of a thin silicon probe that is placed on top of it. Figure 4 introduces the structure. For the VEIM simulations, the calculation of the slab modes is based on a discretization of the slab profile (outside the holes) into 736 linear finite elements; 280 nonuniformly distributed quadratic elements are used to solve the equations along the y-axis.

First we consider the grating without the probe. Since the present method with one mode in the expansion requires a similar computational effort as the Effective Index Method, we compare results of those two methods. As mentioned in Section 2.4, the effective index in a hole in the structure is not uniquely defined, since no guided mode exists there. Therefore, we choose three values that seem reasonable — the highest local refractive index 1.445 (the substrate), the lowest refractive index 1.0 (air), and an in-between value of 1.2. Figure 5 shows the transmission and reflection spectra resulting from these choices in a standard EIM, results from our VEIM with 1 and 80 modes in the expansion, and finally, as a reference, spectra calculated using the QUEP method [37].

The VEIM, $m = 80$ results virtually coincide with the reference results. Using only one mode in the expansion (VEIM, $m = 1$) shifts the spectrum to lower wavelengths and removes the loss mechanisms from the simulations, so the peak in the spectrum is more pronounced, and the reflection and transmission add up to unity. The EIM results are likewise lossless, and their spectra are all shifted to higher wavelengths — and the spectral peaks for all reasonable values of the effective

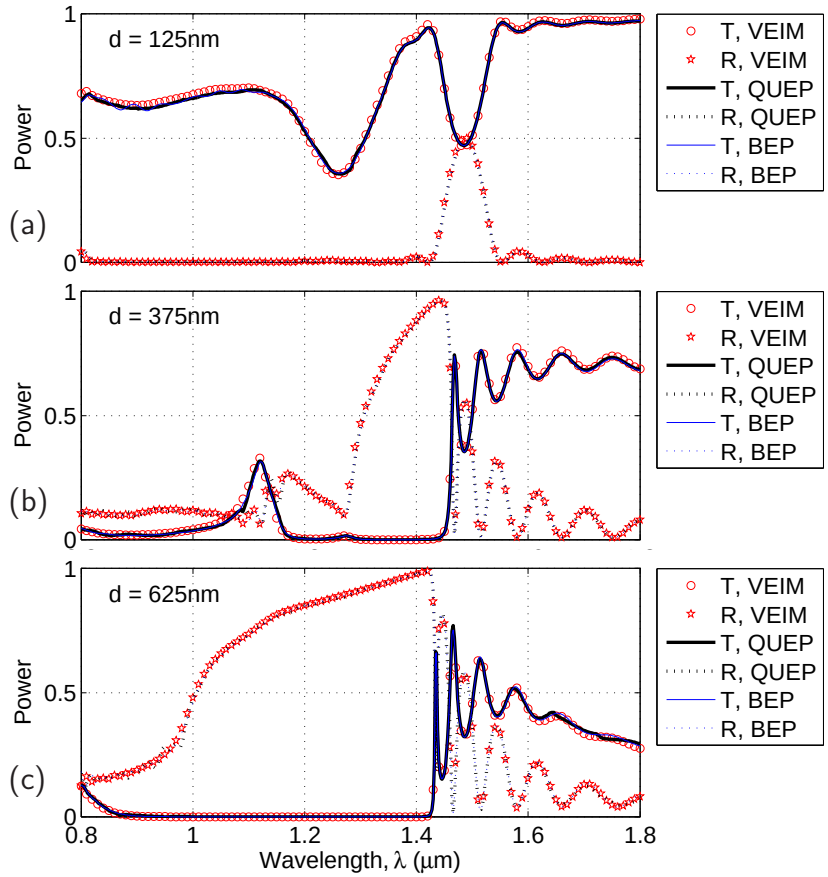

Figure 3: Spectral propagation properties, modal reflection R and transmission T, for the grating of Figure 2, calculated by three modelling methods. Groove depth d: (a) $125nm$, (b) $375nm$ and (c) $625nm$.

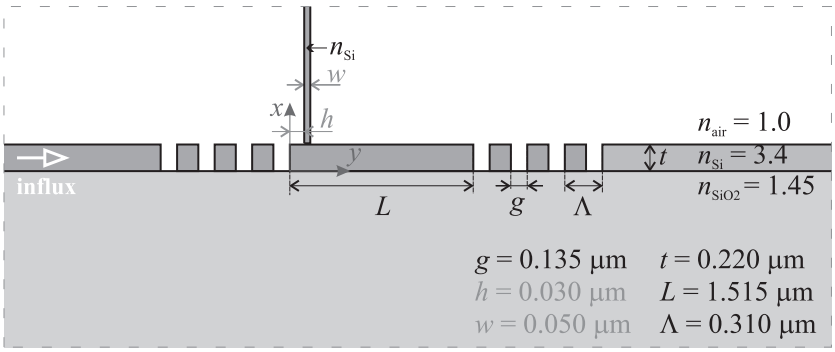

Figure 4: A waveguide Bragg grating with defect, perturbed by a thin vertical Si probe, from Ref. [38].

index in the hole regions are displaced from the reference results much further than the VEIM, $m = 1$ results.

To investigate how many modes are needed to accurately simulate a structure like this grating, we perform a convergence analysis in the number of modes in the expansion. We choose a wavelength of $1.54\mu m$, which lies on the flank of the resonance; this is where the sensitivity of transmission and reflection to numerical errors is expected to be the highest. Figure 6 shows the results. Starting from 40 modes, the levels are quite stable already, and at 80 modes we may consider the calculations to be converged.

Figure 7 shows field plots of the grating at the resonance wavelength of $1.5387\mu m$, for VEIM expansions with one, ten and eighty modes. With one mode, there is no radiation, and the transmission is low. Using ten modes already allows for significant radiation, but the reflection and transmission values are still relatively far from the converged values.

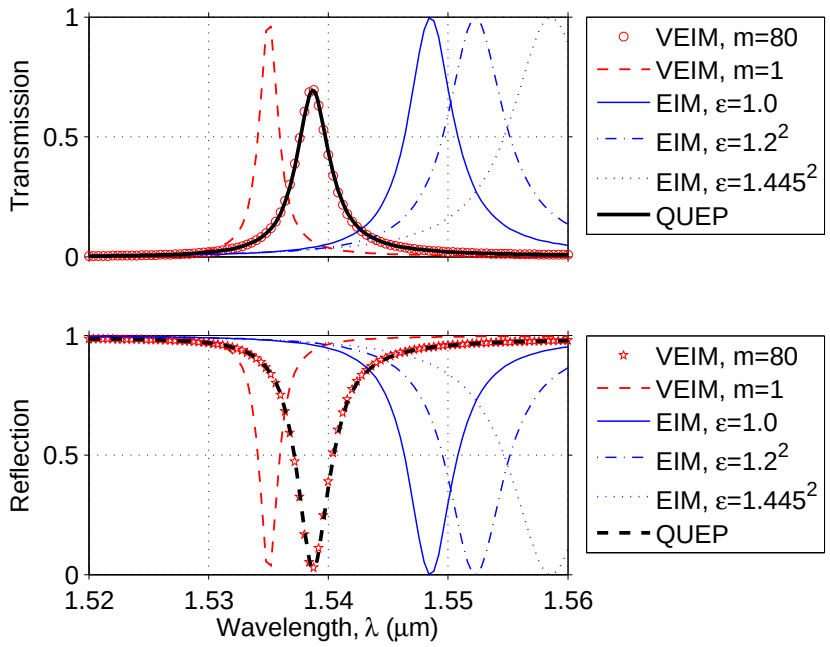

Figure 5: Resonant transmission through the defect grating of Figure 4, for different computational methods.

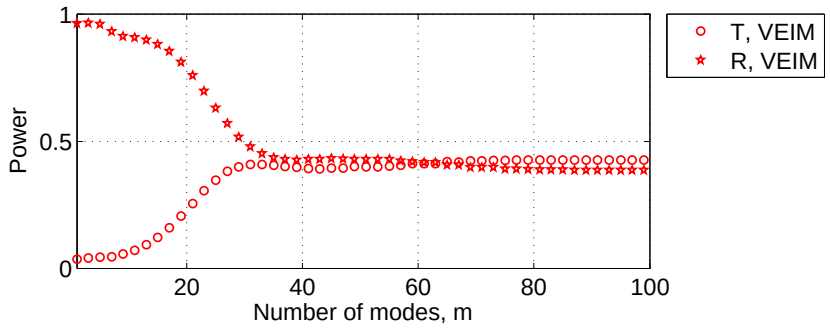

Figure 6: Convergence of transmission T and reflection R at wavelength $\lambda = 1.54\mu m$ versus the number of modes m in VEIM simulations of the grating of Figure 4, for absent tip.

When the defect cavity is perturbed with a silicon probe, the spectrum shifts and deforms. Figure 8 shows the transmission spectrum with the probe, placed near one end of the cavity, as indicated in Figure 4. Again, the VEIM results are very close to the reference QUEP data. Figure 9 shows the field for the structure with the tip at a wavelength of $1.5387\mu m$, the resonance wavelength of the unperturbed structure. The field clearly is disturbed strongly. Remarkably, one can see the fundamental mode of the silicon probe running upward - even though the present method essentially only propagates modes horizontally. The PMLs allow for radiation to leave the domain vertically.

3.3 Taper

Our last example is the vertical taper of Figure 10. We are interested in the transmission from the fundamental mode of the left-hand waveguide to the fundamental mode of the thicker right-hand waveguide.

As discussed in Section 2.3.1, in order to properly influx a mode, and also to analyze the outgoing power of a mode, it is beneficial to have those modes in the expansion of the vertical field. Therefore, we expand the field into a number of modes of the left-hand waveguide plus the fundamental mode of the right-hand guide. The maximum PML strength is set to $\sigma_{max} = 0.6$. The vertical basis modes are calculated using 368 linear finite elements; 608 quadratic elements discretize the horizontal computational window. Figure 11 shows the absolute value of the E_z field for the present method,

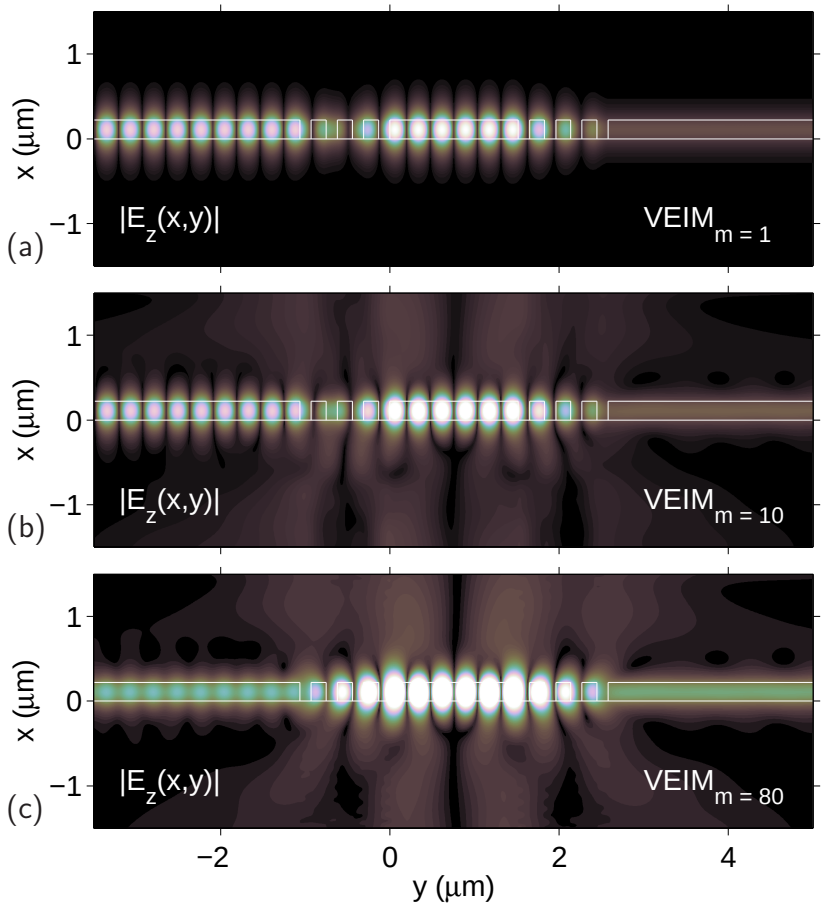

Figure 7: Absolute value of the field profile E_z for the grating of Figure 4, without the tip, at the resonance wavelength $\lambda = 1.5387\mu m$. (a) a VEIM simultion with only one mode in the expansion; (b) VEIM expansion with 10 modes; (c) the converged results for 80 modes.

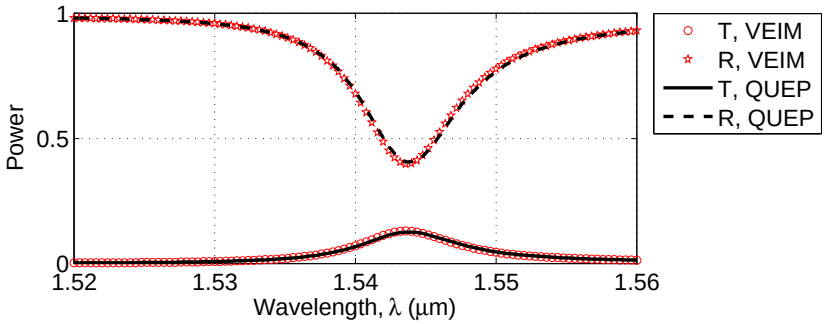

Figure 8: Spectral transmission T and reflection R through the defect grating of Figure 4 if the probe is present. VEIM and QUEP results are compared.

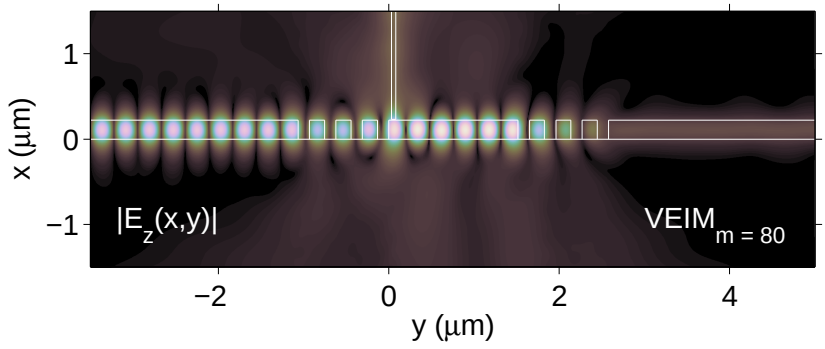

Figure 9: Absolute value of the field profile E_z of the grating of Figure 4 with the probe on top, at the resonance wavelength $\lambda = 1.5387\mu m$. The probe switches the device to a low-transmission state.

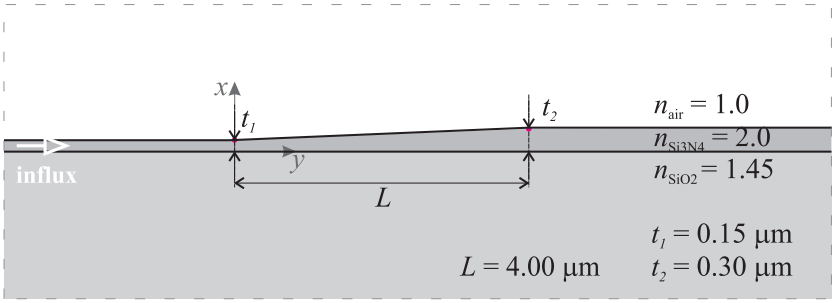

Figure 10: A vertical taper in Si_3N_4 on SiO_2 with air cladding, simulated at a wavelength of $1.55\mu m$. The taper is $4\mu m$ long and tapers linearly from 150 to $300nm$ thickness.

with only 10 modes from the left waveguide, together with rigorous numerical results, obtained with the Finite-Difference-Time-Domain (FDTD) solver from a commercial package [39]. Even for such a low number of modes in the expansion, the fields match remarkably well.

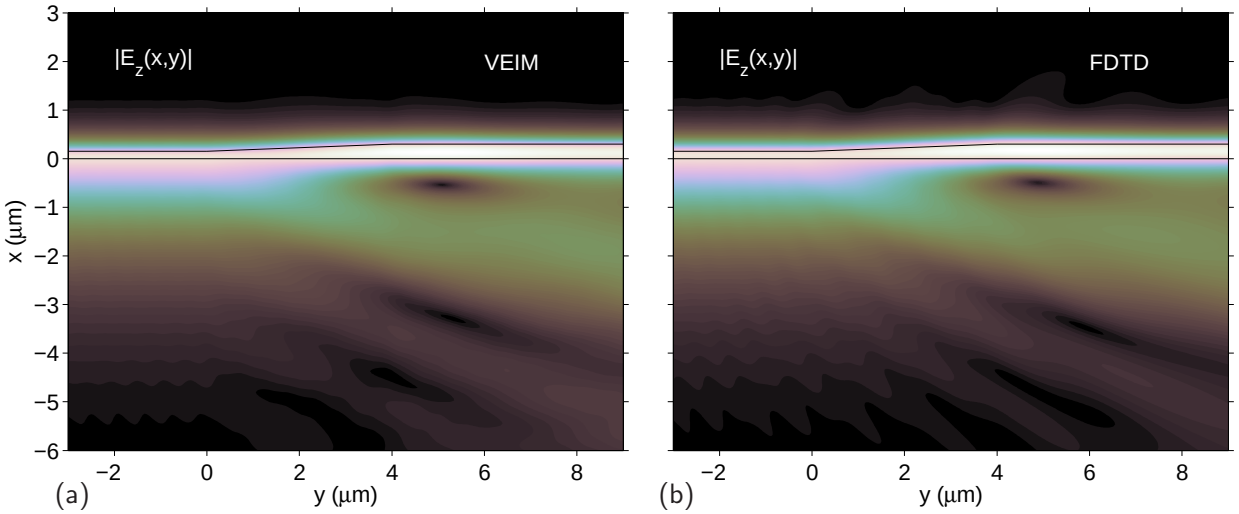

Figure 11: Absolute value of the field profile E_z of the vertical taper of Figure 10. (a) The present method, a VEIM expansion with 10 modes from the left (thin) guide, and 1 mode from the right (thick) one. (b) FDTD reference results.

Results of a convergence analysis for the taper structure are given in Figure 12. We take one mode of the right-hand waveguide in the expansion and vary the number of modes m from the left-hand waveguide. Already with 6 modes from the left-hand guide the result is well within 1% of the reference results, and with 10 modes the transmission can be said to be converged.

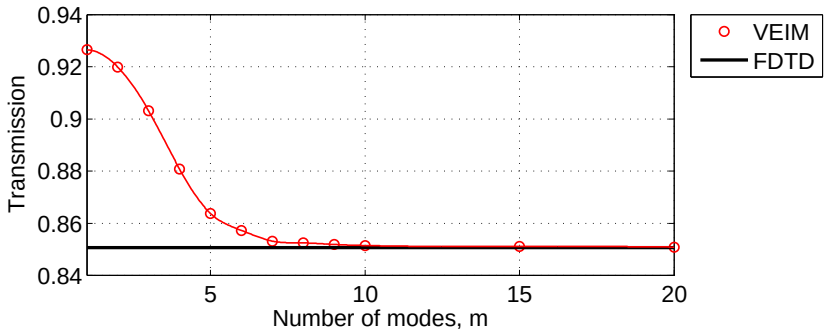

Figure 12: VEIM simulations of the taper of Figure 10, convergence: The plot shows the guided wave transmission versus the number of modes from the thin waveguide in the VEIM expansion. The thicker waveguide contributes one mode to the expansion.

4 Concluding remarks

The VEIM algorithm, as proposed in this paper, constitutes a viable alternative to established quasi-analytical solvers for optical Helmholtz problems, so far in 2D. In particular, the method has similarities to and improves upon the popular EIM and BEP schemes: As in a standard EIM (though with less heuristics involved), rough approximations can be obtained through expansions with one or only very few terms, at very low computational cost. In an intermediate regime already quite acceptable results emerge with only a very moderate number of expansion terms, as shown in some of our examples. VEIM calculations with a larger number of basis modes yield converged results, just as the established BEP schemes. Contrary to the BEP method with PML's, however, our solutions are continuous everywhere; no discontinuities appear on the interfaces between slices, which is a problem for BEP especially when using a low number of modes, and the peaks near the PML boundaries that can appear in standard BEP [40] have not been observed in the current results.

As an alternative to the numerical solution presented here, a semi-analytic solution method for structures with piecewise constant rectangular refractive index distributions could be established, that might be more efficient than the present numerical implementation of the algorithm for those specific cases.

The present numerical variant, however, also serves to obtain experiences for an extension of the approach towards 3D. After a dimensionality reduction using vectorial slab modes, systems of partial differential equations emerge in two spatial dimensions, which require a numerical treatment anyway. Preliminary results have been reported in Ref. [41].

Acknowledgements

This work was supported by the Dutch Technology Foundation (BSIK / NanoNed project TOE.7143)

References

[1] K. S. Chiang. Analysis of optical fibers by the effective-index method. *Applied Optics*, 25(3):348–354, 1986.

[2] K. van de Velde, H. Thienpont, and R. van Geen. Extending the effecive index method for arbitrary shaped inhomogeneous optical waveguides. *Journal of Lightwave Technology*, 6(6):1153–1159, 1988.

[3] C. Vassallo. *Optical waveguide concepts*. Elsevier, Amsterdam, 1991.

[4] T. M. Benson, R. J. Bozeat, and P. C. Kendall. Rigorous effective index method for semiconductor rib waveguides. *IEE Proceedings*, 139(1):67–70, 1992.

[5] R. März. *Integrated optics – design and modelling*. Artech house, Boston, London, 1994.

[6] K. S. Chiang. Analysis of the effective-index method for the vector modes of rectangular-core dielectric waveguides. *IEEE Transactions on Microwave Theory and Technology*, 44(5):692–700, 1996.

[7] K. Okamoto. *Fundamentals of Optical Waveguides*. Academic Press, SanDiego, 2000.

[8] J. Čtyroký. Photonic bandgap structures in planar waveguides. *Journal of the Optical Society of America A*, 18(2):435–441, 2001.

[9] M. Qiu, K. Azizi, A. Karlsson, M. Swillo, and B. Jaskorzynska. Numerical studies of mode gaps and coupling efficiency for line-defect waveguides in two dimensional photonic crystals. *Physical Review B*, 64:155113–1–5, 2001.

[10] J. Witzens, M. Lončar, and A. Scherer. Self-collimation in planar photonic crystals. *IEEE Journal of Selected Topics in Quantum Electronics*, 8(6):1246–1257, 2002.

[11] S. Shi, C. Chen, and D. W. Prather. Revised plane wave method for dispersive material and its application to band structure calculations of photonic crystal slabs. *Applied Physics Letters*, 86:043104–1–3, 2005.

[12] M. Hammer and O. V. Ivanova. Effective index approximations of photonic crystal slabs: a 2-to-1-D assessment. *Optical and Quantum Electronics*, 2009. (accepted).

[13] G. Sztefka and H. P. Nolting. Bidirectional eigenmode propagation for large refractive index steps. *IEEE Photonics Technology Letters*, 5(5):554–557, 1993.

[14] J. Willems, J. Haes, and R. Baets. The bidirectional mode expansion method for two-dimensional waveguides: the TM case. *Optical and Quantum Electronics*, 27:995–1007, 1995.

[15] M. Lohmeyer and R. Stoffer. Integrated optical cross strip polarizer concept. *Optical and Quantum Electronics*, 33(4/5):413–431, 2001.

[16] P. Bienstmann and R. Baets. Advanced boundary conditions for eigenmode expansion models. *Optical and Quantum Electronics*, 34(5/6):523–540, 2002.

[17] M. Lohmeyer. Mode expansion modeling of rectangular integrated optical microresonators. *Optical and Quantum Electronics*, 34(5):541–557, 2002.

[18] O. V. Ivanova, M. Hammer, R. Stoffer, and E. van Groesen. A variational mode expansion mode solver. *Optical and Quantum Electronics*, 39(10–11):849–864, 2007.

[19] O. V. Ivanova, R. Stoffer, and M. Hammer. A variational mode solver for optical waveguides based on quasi-analytical vectorial slab mode expansion. *Optics Communication*, 2009. (submitted).

[20] W. Chew, J. Jin, and E. Michielssen. Complex coordinate stretching as a generalized absorbing boundary condition. *Microwave and Optical Technology Letters*, 15(6):363–369, 1997.

[21] E. W. C. van Groesen and J. Molenaar. *Continuum modeling in the physical sciences*. SIAM, USA, 2007.

[22] COMSOL. `http://www.comsol.com`.

[23] J. B. Nicolau and E. van Groesen. Hybrid analytic-numeric method for light through a bounded planar dielectric domain. *Journal of Nonlinear Optical Physics and Materials*, 14(2):161–176, 2005.

[24] A. Sopaheluwakan. *Characterization and simulation of Localized states in optical structures*. PhD thesis, University of Twente, The Netherlands, 2006.

[25] R. Stoffer, A. Sopaheluwakan, M. Hammer, and E. van Groesen. Helmholtz solver with transparent influx boundary conditions and nonuniform exterior. In *Proc. of XVI International Workshop on Optical Waveguide Theory and Numerical Modelling*, Copenhagen, Denmark, 2007. book of abstracts 3.

[26] J. Čtyroký. Improved bidirectional-mode expansion propagation algorithm based on fourier series. *Journal of Lightwave Technology*, 25(9):2321–2330, 2007.

[27] O. V. Ivanova, R. Stoffer, and M. Hammer. A dimensionality reduction technique for scattering problems in photonics. In *Proc. of 1st International Workshop on Theoretical and Computational Nano-Photonics*, Bad Honnef, Germany, 2008.

[28] E. van Groesen. Variational modelling for integrated optical devices. Seminar Mathematical Physics, University of Twente, Enschede, The Netherlands, 23 September 2002.

[29] J.-P. Berenger. A perfectly matched layer for the absortion of electromagnetic waves. *Journal of Computational Physics*, 114(2):185–200, 1994.

[30] W. C. Chew and W. H. Weedon. A 3D perfectly matched medium from modified Maxwell's equations with stretched coordinates. *Microwave and Optical Technology Letters*, 7(13):590–604, 1994.

[31] S. B. Gaál, H. J. W. M. Hoekstra, and P. V. Lambeck. Determining PML modes in 2D stratified media. *Journal of Lightwave Technology*, 21(1):293–298, 2003.

[32] M. Hammer. Hybrid analytical/numerical coupled-mode modeling of guided wave devices. *Journal of Lightwave Technology*, 25(9):2287–2298, 2007.

[33] J. Jin. *The Finite Element Method in Electromagnetics*. Wiley-IEEE Press, New York, 2002.

[34] J. van Kan, G. Segal, and F. Vermolen. *Numerical methods in scientific computing*. VSSD, Delft, The Netherlands, 2005.

[35] M. Hammer and O. V. Ivanova. On effective index approximations of photonic crystal slabs. In *Proc. of 13th Annual Symposium IEEE/LEOS Benelux Chapter*, Enschede, The Netherlands, 2008.

[36] J. Čtyroký, S. Helfert, R. Pregla, P. Bienstman, R. Baets, R. de Ridder, R. Stoffer, G. Klaasse, J. Petrcek, P. Lalanne, J.-P. Hugonin, and R. M. De La Rue. Bragg waveguide grating as a 1D photonic band gap structure: COST 268 modelling task. *Optical and Quantum Electronics*, 34:455–470, 2002.

[37] M. Hammer. Quadridirectional eigenmode expansion scheme for 2-D modeling of wave propagation in integrated optics. *Optics Communication*, 235(4), 2004.

[38] W. L. C. Hopman, R. Stoffer, and R. M. de Ridder. High-resolution measurement of resonant wave patterns by perturbing the evanescent field using a nanosized probe in a transmission scanning near-field optical microscopy configuration. *Journal of Lightwave Technology*, 25(7):1811–1818, 2007.

[39] OptoDesigner by PhoeniX Software. `http://www.phoenixbv.com/`.

[40] N. Gregersen and J. Mørk. An improved perfectly matched layer for the eigenmode expansion technique. *Optical and Quantum Electronics*, 40(11–12):957–966, 2008.

[41] O. V. Ivanova, R. Stoffer, L. Kauppinen, and M. Hammer. Variational effective index method for 3D vectorial scattering problems in photonics: TE polarization. In *Proc. of Progress In Electromagnetics Research Symposium*, Moscow, Russia, 2009.